656 *Biochemistry* **2010,** *49,* 656–668
DOI: 10.1021/bi901459c

BIOCHEMISTRY
including biophysical chemistry & molecular biology
Article

Kinetic Mechanism of DNA Unwinding by the BLM Helicase Core and Molecular Basis for Its Low Processivity[†]

Ye Yang,[‡] Shuo-Xing Dou,*[,‡] Ya-Nan Xu,[‡,§] Nicolas Bazeille,[∥] Peng-Ye Wang,[‡] Pascal Rigolet,[∥] Hou-Qiang Xu,[∥] and Xu Guang Xi*[,∥]

[‡]*Laboratory of Soft Matter Physics, Beijing National Laboratory for Condensed Matter Physics, Institute of Physics, Chinese Academy of Sciences, Beijing 100190, China,* [§]*Department of Physics, Renmin University, Beijing 100872, China, and* [∥]*CNRS, UMR 2027, Institut Curie—Section de Recherche, Centre Universitaire, Bâtiment 110, F-91405 Orsay, France*

Received August 19, 2009; Revised Manuscript Received November 5, 2009

ABSTRACT: Bloom's syndrome (BS) is a rare human autosomal recessive disorder characterized by a strong predisposition to a wide range of cancers commonly affecting the general population. Understanding the functioning mechanism of the BLM protein may provide the opportunity to develop new effective therapy strategies. In this work, we studied the DNA unwinding kinetic mechanism of the helicase core of the BLM protein using various stopped-flow assays. We show that the helicase core of BLM unwinds duplex DNA as monomers even under conditions strongly favoring oligomerization. An unwinding rate of ~20 steps per second and a step size of 1 bp have been determined. We have observed that the helicase has a very low processivity. From dissociation and inhibition experiments, we have found that during its ATP hydrolysis cycle in DNA unwinding the helicase tends to dissociate from the DNA substrate in the ADP state. The experimental results imply that the BLM helicase core may unwind duplex DNA in an inchworm manner.

Bloom's syndrome (BS) [1] is an inherited autosomal recessive disorder whose clinical manifestation includes severe pre- and postnatal growth retardation, variable degrees of immunodeficiency, photosensitivity, and increased susceptibility to neoplasms of many sites and types (*1*). At the cellular level, one hallmark of BS is an increase in various types of chromosomal abnormalities, including mutations and elevated frequency of chromosome breaks and exchanges, especially a high level of sister-chromatid exchanges (*2*, *3*).

The gene defective in BS, *BLM*, is located on chromosome 15 at 15q26.1, adjacent to the FES protooncogene. The product of the *BLM* gene is a 1417 amino acid protein which shares amino acid sequence similarity with a number of highly conserved RecQ family helicases (*4*). The BLM protein contains a central region homologous to that of the RecQ subfamily of DExH box-containing DNA helicases. In addition to the central helicase domain, BLM possesses a C-terminal region that contains an additional conserved RQC domain (RecQ conserved) including the nucleolar targeting sequence and a zinc-binding motif (*5*, *6*), which is essential for enzymatic activities and protein folding (*7*). The BLM N-terminus lacks homology with any other identified proteins or motifs. The N-terminal residues are involved in interactions with other proteins (*3*). It appears that they do not contribute to the enzymatic activities, since the N-terminal truncated BLM protein displays very similar biochemical properties as the full-length protein (*8*).

Biochemical studies have shown that the BLM protein unwinds a wide variety of different oligonucleotide-based DNA substrates, including the duplex with a 3′ ssDNA overhang, the forked duplex, and the joint DNA molecule (D-loops) (*9*). BLM protein also promotes branch migration of a Holliday junction (*10*) and resolves double Holliday junction with topoisomerase III (*11*) and BLAP75 (*12*). These data support the hypothesis that the BLM protein is active in DNA repair processes that are involved in DNA recombination. In accordance with the above functions, we have observed in our previous preliminary study that both the full-length BLM protein and its helicase core unwind duplex DNA inefficiently, very probably due to a limited processivity. To better understand the DNA unwinding behaviors of the BLM helicase, the actual processivity as well as the molecular basis for it are worth determining.

Previously, electron microscopy study has demonstrated that the full-length recombinant BLM protein forms hexameric ring structures (*13*). However, size-exclusion chromatography and DNA unwinding characterizations have shown that the catalytically active, truncated BLM helicase core ($BLM^{642-1290}$) was monomeric in solution and lacked cooperativity in helicase reaction with respect to ATP concentration (*8*). Usually, the isolated subunits of an oligomeric helicase are inactive (*14*, *15*). But why does the isolated helicase core of the hexameric BLM protein unwind DNA as a monomer? For further understanding the mechanism of DNA unwinding by the BLM helicase core, its functional form merits further clarification. Moreover, although a number of experiments were performed to characterize the BLM protein's potential physiological DNA substrates by *in vitro* studies, little is known about its fundamental helicase properties, such as its DNA unwinding rate and step size.

[†]This work was supported by the National Natural Science Foundation of China, the 973 Project, Shanghai Municipal Science and Technology Commission (No. 07DZ22940), Shanghai Municipal Wildlife Administration (No. SBHZ2006_01), and the Institut Curie and the Centre National de la Recherche Scientifique (CNRS).

*To whom correspondence should be addressed. S.-X.D.: e-mail, sxdou@aphy.iphy.ac.cn; tel, +86 10 8264 9484; fax, +86 10 8264 0224. X.G.X.: e-mail, xu-guang.xi@curie.u-psud.fr; tel, +33 1 6986 3181; fax, +33 1 6986 9429.

[1]Abbreviations: BS, Bloom's syndrome; ssDNA, single-stranded DNA; dsDNA, double-stranded DNA.

 Published on Web 12/22/2009

In the present study, we utilized fluorometric assays to study BLM-catalyzed unwinding of duplex DNA in real time under various experimental conditions. The work was carried out with the helicase core of BLM protein, consisting of the seven helicase motifs, the RQC and HRDC domains (amino acid residues from 642 to 1290). We have performed pre-steady-state, single- and multiple-turnover kinetic studies using different DNA substrates. We show that the BLM helicase core unwinds duplex DNA as monomers under all of the conditions investigated. The unwinding rate, step size, and processivity have been determined. The low processivity of the helicase is found to originate from the ADP state in which the helicase binds weakly to the DNA substrate. Implications of the results for the DNA unwinding mechanism of the helicase are discussed.

EXPERIMENTAL PROCEDURES

Reagents and Buffers. All chemicals were of reagent grade and all buffers were prepared in high quality deionized water from Milli-Q ultrapure water purification systems (Millipore, France) having resistivity greater than 18.2 MΩ·cm. All unwinding reactions and DNA-binding assays were performed in buffers containing 25 mM Tris-HCl (pH 7.5 at 25 °C), 100 mM NaCl, 1 mM $MgCl_2$, and 3 mM DTT, unless noted elsewhere. ATP was from Sigma (St. Louis, MO) and was dissolved as a concentrated stock at pH 7.0. ATP concentration was determined by using an extinction coefficient at 259 nm of 1.54×10^4 cm^{-1} M^{-1}.

BLM Helicase and Oligonucleotide Reaction Substrates. The helicase core of the BLM protein, $BLM^{642-1290}$, was prepared as described (*5*). The dsDNA substrates used in the unwinding assays have both strands labeled with fluorescein (F) and hexachlorofluorescein (H), respectively. Their structures and sequences, the same as that in our previous studies (*16*), are shown in Table 1. The protein trap used for single-turnover kinetic experiments is 56-nt poly(dT), dT_{56}. Single-stranded oligonucleotides, with or without fluorescent labels, were purchased from Shanghai Sangon Biological Engineering Technology and Services Co., Ltd. (Shanghai, China), and all of the synthetic oligonucleotides were purified by high-performance liquid chromatography before storage in 10 mM Tris-HCl (pH 8.0) and 1 mM EDTA at −20 °C. Concentrations of single-stranded oligodeoxynucleotides were determined spectrophotometrically based on extinction coefficients calculated by the nearest-neighbor method. A 50 μM working stock of dsDNA was prepared by mixing equal concentrations of complementary single-stranded oligonucleotides in a 20 mM Tris-HCl buffer (pH 8.0 at 25 °C) containing 100 mM NaCl, followed by heating to 90 °C. After equilibrating for 3 min, annealing was allowed by slow cooling to room temperature. The duplex was stored at −20 °C.

Fluorometric Titration Assays. DNA binding of the BLM helicase core was analyzed by fluorescence polarization as described previously (*16*, *17*). The assay was performed using a Bio-Logic autotitrator (TCU-250) and a Bio-Logic optical system (MOS450/AF-CD) in fluorescence anisotropy mode. Varying amounts of proteins were added to 1 mL of binding buffer containing 2 nM DNA substrate. Each sample was allowed to equilibrate in solution for 1.5 min, after which fluorescence polarization was measured. Titrations were performed in a temperature-controlled cuvette at 25 °C. The solution was stirred continuously by a small magnetic stir bar during the whole titration process.

The stoichiometry (N) and dissociation constant (K_d^{DNA}, in units of molarity) were determined by globally fitting the anisotropy data according to eq 1

$$A = A_{min} + (A_{max} - A_{min})\frac{\Delta - \sqrt{\Delta^2 - 4N[S_T][E_T]}}{2N[S_T]} \quad (1)$$

where A is the fluorescence anisotropy at a given enzyme concentration, A_{max} is the anisotropy at saturation, A_{min} is the initial anisotropy, $\Delta = N[S_T] + [E_T] + K_d^{DNA}$, $[S_T]$ is the concentration of DNA substrate and $N[S_T]$ the concentration of total binding sites for the helicase, and $[E_T]$ is the total concentration of the enzyme in the binding solution.

The fluorometric mantATP-binding assay was also performed using the Biologic autotitrator; 0.2 μM protein in 1 mL of reaction buffer in a $10 \times 10 \times 40$ mm^3 quartz cuvette was used. The protein solution was titrated with mantATP, during which the protein was excited at 280 nm and the fluorescence of mantATP at 440 nm due to fluorescence resonance energy transfer (FRET) was measured. The apparent dissociation constant K_d^{ATP} was determined by fitting the fluorescence intensity (corrected for the inner filter effect and dilution effect (*18*)) to the rigorous eq 2

$$F = F_s + f_d x + (f_c - f_d)\frac{(x + 0.2 + K_d^{ATP}) - \sqrt{(x+0.2+K_d^{ATP})^2 - 0.8x}}{2} \quad (2)$$

where F_s is the starting fluorescence of the reaction mixture, f_d is the fluorescence coefficient of free mantATP, f_c is the fluorescence coefficient of complex formed, and x is the total concentration of mantATP.

Stopped-Flow Kinetic Study. All of the stopped-flow kinetic assays were carried out using a Bio-Logic SFM-400 mixer

Table 1: Substrates Used in Unwinding Assays

substrate	structure and sequence
16-bp duplex with 3′-ssDNA tail	3′-F-TTAGGCAGCTCGTCTC-5′ [a] 5′-H-AATCCGTCGAGCAGAG(dT_N)-3′ [b]
12-bp duplex with 10-nt 3′-ssDNA tail	3′-F-GCAGCTCGTCTC-5′ 5′-H-CGTCGAGCAGAG(dT_{10})-3′
20-bp duplex with 10-nt 3′-ssDNA tail	3′-F-CGGAGCGACGGCAGCGGTTT-5′ 5′-H-GCCTCGCTGCCGTCGCCAAA(dT_{10})-3′
25-bp duplex with 10-nt 3′-ssDNA tail	3′-F-CGGAGCGACGGCAGCGGTTTGCTTC-5′ 5′-H-GCCTCGCTGCCGTCGCCAAACGAAG(dT_{10})-3′

[a] F, fluorescein. [b] H, hexachlorofluorescein.

with a 1.5 mm × 1.5 mm cell (FC-15, Bio-Logic) and the above Bio-Logic MOS450/AF-CD optical system equipped with a 150 W mercury−xenon lamp.

In the DNA unwinding assays, fluorescein was excited at 492 nm (2 nm bandwidth), and its emission was monitored at 525 nm using a high-pass filter with 20 nm bandwidth (D525/20, Chroma Technology Co., Bellows Falls, VT). Pre-steady-state and single-turnover unwinding kinetics were measured in a two-syringe mode, where the helicase and duplex DNA substrates were preincubated at 25 °C in syringe 1 for 5 min while ATP and the protein trap were preincubated in syringe 4 (see Figure S1 in the Supporting Information). Each syringe contained unwinding reaction buffer, and the unwinding reaction was initiated by rapid mixing of the two syringes. All concentrations listed are after mixing unless noted otherwise. For converting the output data from volts to fraction of DNA unwound, a calibration experiment was performed in a four-syringe mode, where helicase in syringe 1, H-labeled ss oligonucleotides in syringe 2, and F-labeled ss oligonucleotides in syringe 3 were incubated in unwinding reaction buffer while ATP and the protein trap were incubated in syringe 4. The fluorescent signal of the mixed solution in equilibrium from the four syringes corresponded to 100% unwinding.

Multiple-turnover unwinding kinetics was measured in the same way as the single-turnover kinetics. The only difference was that no protein trap was used.

For the kinetic assay of helicase dissociation from DNA substrate, the helicase was preincubated with the DNA substrate (labeled only with fluorescein) in syringe 1 while a protein trap with or without nucleotide cofactors (AMPPNP and ADP) was in syringe 4. The reaction was initiated by rapid mixing of the two syringes. The sample was excited at 492 nm, and the anisotropy was monitored at 525 nm. The decreasing of fluorescence anisotropy reflected the helicase dissociation process. In the special case of nucleotide cofactor ADP·MgF_3, the helicase was preincubated with the DNA substrate in the $MgCl_2$-containing buffer in the presence of NaF in syringe 1, thus allowing enough formation time for the BLM−ADP·MgF_3−DNA ternary complex.

All of the solutions in the kinetic studies were filtered and extensively degassed immediately before they were used. The stopped-flow temperature was controlled by means of an external thermostated water bath (B12; Thermo Haake) and a high flux pump to circulate the water between the bath and the stopped-flow apparatus. The reaction temperature was 25 °C unless noted otherwise.

Kinetic Data Analysis. All stopped-flow kinetic traces were an average of at least 10 individual traces. The kinetic traces were analyzed using Bio-Kine (version 4.26; Bio-Logic) with multi-exponential functions or with eq 3:

$$A(t) = A\left(1 - \sum_{r=1}^{n} \frac{k_{obs}^{r-1} t^{r-1}}{(r-1)!} e^{-k_{obs} t}\right) \quad (3)$$

Equation 3 was used to determine the number of steps (n) required for unwinding the duplex DNA as well as the unwinding rate in each step (*19*, *20*). A is the unwinding amplitude, $k_{obs} = k_u + k_d$ is the observed rate constant for each unwinding step with k_u being the net rate constant for each step and k_d the dissociation rate in each step.

RESULTS

Determination of the ssDNA Binding Stoichiometry. As in the case of the *Escherichia coli* RecQ helicase (*21*), a 3′-ssDNA-tailed duplex DNA is a good substrate for efficient unwinding by BLM (*8*, *22*). Before carrying out kinetic analyses of the DNA unwinding behaviors of the helicase, we need to know its binding site size on ssDNA. Previously, we have determined the binding site size of *E. coli* RecQ on ssDNA as ∼9 nt by using a fluorescence anisotropy assay (*16*). As the BLM helicase core and *E. coli* RecQ display high sequence and structural similarities (*6*), we expect that the BLM helicase core may have a similar binding site size. To verify this, we carried out fluorescence anisotropy assays for the helicase. The titration experiments were performed under conditions essentially identical to those used for DNA unwinding, but without ATP, by titrating 2 nM fluorescein-labeled 22-nt ssDNA (initial concentration) with increasing helicase concentration. The resulting binding isotherm was fitted with eq 1 to determine the stoichiometric number (N) and the dissociation constant (K_d^{DNA}) (Figure 1). From $N = 2.9 \pm 0.4$ and the ssDNA length (22 nt) we obtained a binding site size of 7.6 ± 1.1 nt, which is indeed similar to that determined for RecQ. The dissociation constant for helicase binding to a single binding site on DNA is $K_d^{DNA} = 2.3 \pm 0.6$ nM.

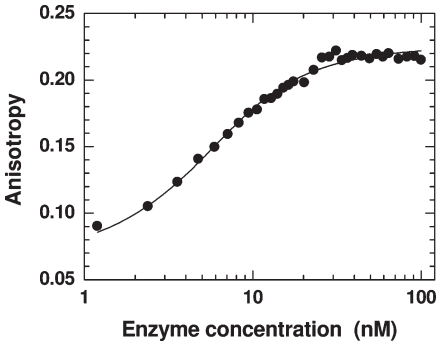

FIGURE 1: The anisotropy-based DNA-binding isotherm. The fluorescence anisotropy value was determined as a function of the enzyme concentrations for a fluorescein-labeled 22-mer ssDNA substrate. 2 nM fluorescein-labeled ssDNA was titrated with the BLM helicase core under conditions as described in Experimental Procedures. The solid line represents the best fit of the data to eq 1. The determined stoichiometry and dissociation constant are $N = 2.9 \pm 0.4$ and $K_d^{DNA} = 2.3 \pm 0.6$ nM. The errors here and elsewhere in all of the work were obtained from fittings of data curves.

Pre-Steady-State Kinetic Analysis of DNA Unwinding. To determine the oligomeric state of the helicase in DNA unwinding, we first carried out pre-steady-state kinetic studies. Under appropriate steady-state conditions without a protein trap, we can measure the first cycle of DNA unwinding reaction (i.e., pre-steady-state burst), the behavior of which is determined by the oligomeric state of the helicase. This method has been used frequently in studying DNA unwinding activity and the kinetic mechanism of different helicases such as Dda (*23*), bacteriophage T7 helicase (*24*), TraI (*25*), and RecQ (*16*).

In steady-state experiments, a pre-steady-state burst will be observed as long as the processivity of unwinding activity of the helicase is sufficiently high such that significant unwinding will occur before the onset of steady-state behavior (resulting from the dissociation and rebinding of helicase from/to the unwinding substrate). Furthermore, as the burst amplitude of DNA unwound will be proportional to the concentration of initial productive helicase/DNA complex, the ideal condition for observing a pre-steady-state burst will be that most helicase molecules bind to the DNA substrate before initiation of DNA unwinding. This requires that the DNA concentration exceeds that of the helicase as well as the value of the dissociation

constant. Therefore, we used a DNA concentration of 60 nM with lower helicase concentrations.

The DNA substrate we have chosen to use is a 10-nt-tailed 12-bp ss/dsDNA. From the ssDNA binding size just determined, we know that the helicase binds to this DNA substrate approximately with a stoichiometry of one molecule for each DNA substrate, even at a saturating enzyme concentration.

Before carrying out systematic measurements, we need to verify whether a fast phase can be observed that really reflects the first cycle of the unwinding reaction. Thus we first performed the pre-steady-state measurements both without and with a protein trap while using an enzyme concentration of 40 nM. Under the condition without a protein trap, the unwinding kinetic course was composed of two phases: burst and steady-state phases (Figure 2A). By fitting the data between 0 and 0.5 s to eq 3 with $n = 5$ (see the step-size determination section), we obtained both the burst amplitude and the unwinding rate constant as $A = 23.4$ nM and $k_{obs} = 17.5\ s^{-1}$. It should be noted that we have chosen the data points in the 0−0.5 s range for the fitting because this gave the best overlap between the experimental data and the theoretical fitting curves.

In the control experiment with a protein trap (30 μM dT_{56}), only a burst phase was observed in the unwinding kinetics, and the steady-state phase disappeared (Figure 2A). This was expected because the steady-state phase resulted from unwinding activity of the helicase molecules after finishing the reactions in the burst phase and thus was diminished when the trap was used. (For verifying the efficiency of the trap, a test was performed and presented in Figure S2 in the Supporting Information.) From fitting of the data to eq 3 with $n = 5$, we obtained $A = 22.0$ nM and $k_{obs} = 16.6\ s^{-1}$. The kinetic parameters obtained in the above two cases are quite similar, indicating the reliability of the pre-steady-state measurements in characterizing the first reaction cycle of DNA unwinding.

Then we performed measurements under the above pre-steady-state conditions while using different enzyme concentrations (7.5−40 nM). We observed that all of the unwinding kinetic courses were composed of a burst phase and a steady-state phase (Figure 2B). From fitting of the data curves with eq 3, we obtained the burst amplitude and unwinding rate constant for each enzyme concentration (Figure 2C,D and Table S1 in the Supporting Information). As can be seen, the burst amplitude was almost linearly proportional to the enzyme concentration (with a slope of ~0.58) and the unwinding rate was constant over the whole concentration range, clearly indicating that the BLM helicase core unwinds the DNA substrates as monomers, independent of the enzyme concentration used. This is also consistent with previous size-exclusion chromatography data suggesting that the helicase exists as a monomer in solution (*8*).

If the helicase functions as dimers or other oligomers, the burst amplitude would generally not be a linear, but rather a sigmoidal function of the enzyme concentration. In addition, the burst amplitude at low enzyme concentrations would be negligibly small because complexes of DNA bound with two or more helicase molecules should be rare under the experimental conditions used (i.e., DNA substrate with a short tail and enzyme concentrations below that of substrate). In the case of dimeric helicases such as UvrD, Rep, and PcrA, DNA unwinding was negligible when the enzyme concentration was less than that of DNA (*20*, *26*, *27*). Note that if the helicase is active as a stable dimer or other oligomer, the burst amplitude would also be

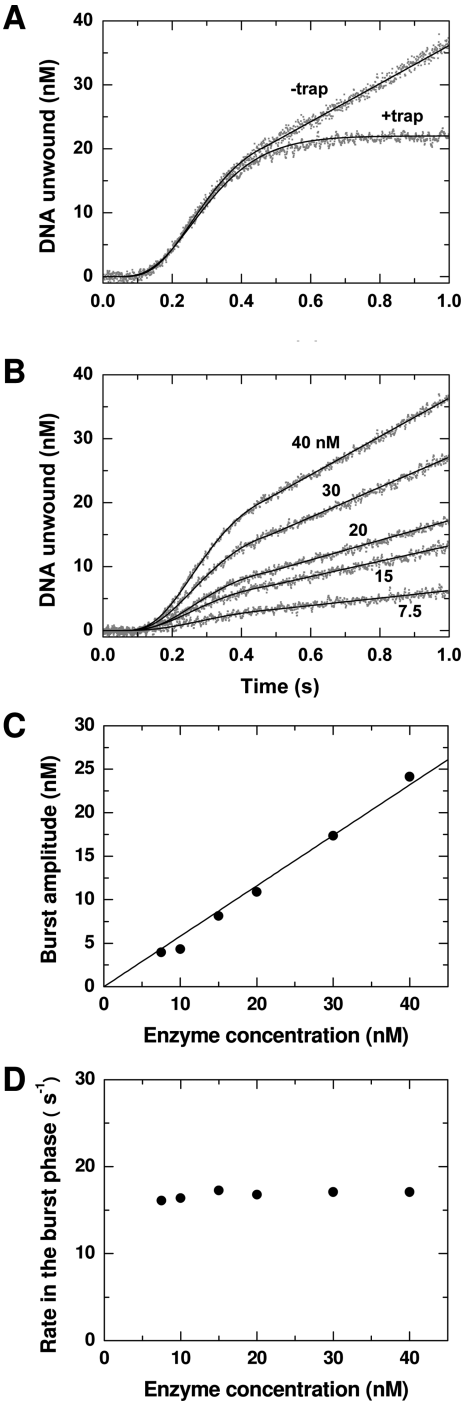

FIGURE 2: DNA unwinding under pre-steady-state conditions. 60 nM 10-nt-tailed 12-bp dsDNA substrate was first preincubated with enzyme at the indicated concentrations in the reaction buffer at 25 °C for 5 min, and the unwinding reaction was initiated by adding 1 mM ATP (see Experimental Procedures). A 30 μM protein trap (dT_{56}) was added together with ATP in the control experiment. As in all of the following cases, the stopped-flow traces represent an average of at least 10 measurements. (A) Kinetic time courses with or without a protein trap. The enzyme concentration was 40 nM in both cases. In the case without a protein trap, the solid line was a best fit of the data to eq 3 for the portion between 0 and 0.5 s with $n = 5$, giving $A = 23.4 \pm 0.2$ nM and $k_{obs} = 17.5 \pm 0.3\ s^{-1}$, and was a fit to a straight line for the later portion (> 0.5 s). In the case with a protein trap (control), the solid line was a best fit of the data to eq 3 with $n = 5$, giving $A = 22.0 \pm 0.1$ nM and $k_{obs} = 16.6 \pm 0.1\ s^{-1}$. (B) Typical kinetic time courses for different enzyme concentrations. The solid lines are fits of the data using the same method as in the case without trap in (A). (C) Amplitude of the burst phase. The solid line is a linear fit of the data with a slope of 0.58 ± 0.02. (D) Unwinding rate for each step in the burst phase. The average value is $16.8 \pm 0.5\ s^{-1}$.

linearly proportional to the enzyme concentration, but the slope could not exceed 0.5.

We found that linear fits of the data points at >0.5 s in the different unwinding curves in Figure 2B produced steady-state rates that were in proportion with the helicase concentrations (data not shown). This indicates that the behavior of the steady-state helicase activity did not vary with the protein concentration, which is expected if the helicase is monomeric.

Ideally, if each helicase monomer binds to a DNA substrate and unwinds the whole duplex of the substrate in the burst phase, the slope of the fitting line in Figure 2C should be close to 1. But the slope obtained is actually ~0.58. Possible reasons for this reduced efficiency include the following: (i) not all enzyme molecules bound to the substrates; (ii) some enzyme molecules dissociated from the substrates upon unwinding initiation; (iii) some enzyme molecules bound to the blunt ends rather than ss/dsDNA junctions of the substrates; (iv) the unwinding processivity of the enzyme was limited. As will be discussed later, the low efficiency resulted mainly from a limited processivity of the helicase.

Multiple-Turnover Kinetics of DNA Unwinding with Substrates of Different 3′-ssDNA Tail Lengths. In the previous pre-steady-state experiments, we have used a subsaturating enzyme concentration. Thus the possibility was not excluded that the BLM helicase core may function as oligomers under conditions allowing oligomerization. Thus we next carried out experiments with saturating helicase and, furthermore, with DNA substrates of various tail lengths (5−50 nt). Depending on the oligomeric state of the helicase, the unwinding behaviors for the different substrates should be similar or quite different. If the helicase only functions as monomers, we expect similar behaviors. Otherwise, distinct behaviors should be observed with the different substrates.

We observed unwinding for all of the DNA substrates. For clarity, only the unwinding kinetic courses for the 5- and 10-nt-tailed substrates are shown (Figure 3A). We found that all of the unwinding kinetics were triphasic and can be well fitted with a triple exponential. The unwinding amplitudes obtained from the fitting were given in Figure 3B. The amplitude for the fast phase A_{fast} was almost independent of the substrate tail length. As at most only one helicase monomer may bind to the short tail of the 5-nt substrate and more than one monomer may bind to the longer tails of the other substrates, the invariability of A_{fast} suggests that the fast phase was only contributed by the helicase monomers bound to the ss/dsDNA junctions.

The rate of the fast unwinding phase, k_{fast}, was given in Figure 3C. k_{fast} was almost constant (~2.3 s^{-1}) for tail lengths longer than 5 nt, further supporting the above suggestion that only helicase monomers bound to the ss/dsDNA junctions contributed to the fast phase. The much lower value of k_{fast} at 5 nt (~0.93 s^{-1}) was due to, as will be discussed later, the low binding affinity of the helicase for this short-tailed substrate.

The above multiple-turnover experimental results thus reveal that the BLM helicase core still catalyzes DNA unwinding as monomers at saturating enzyme concentrations.

In the multiple-turnover kinetic experiments, the unwinding amplitude $A_{slow,1}$ of the first slow phase is negligible for the 5-nt substrate and increases with increasing tail length (Figure 3B). Thus this phase should be mainly contributed by helicase molecules bound to the other positions on the ssDNA tails. As the number of helicase monomers bound to the tails is proportional to the tail length, the amplitude of the first slow phase $A_{slow,1}$ accordingly depends on the tail length.

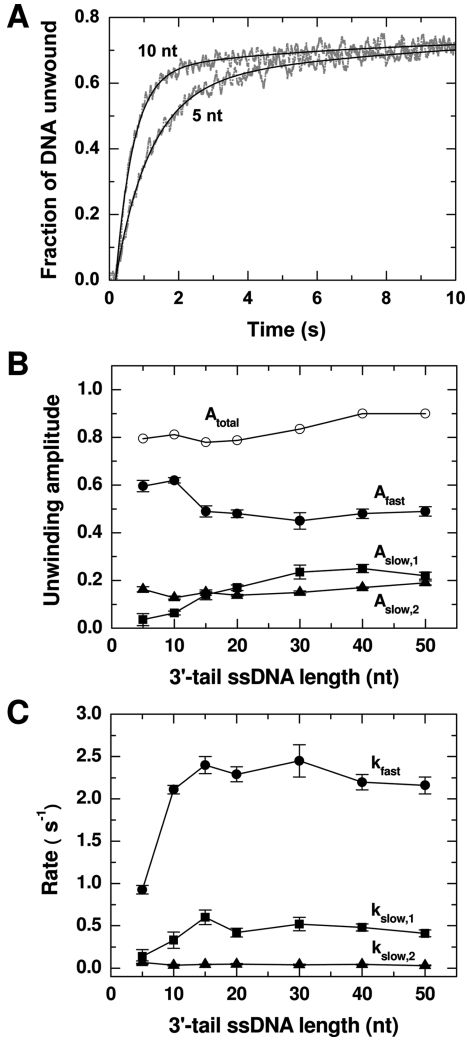

FIGURE 3: Multiple-turnover DNA unwinding for 16-bp duplex DNA substrates of different 3′-ssDNA tail lengths. 2 nM DNA substrate was first preincubated with excess enzyme (80 nM) in the reaction buffer at 25 °C for 5 min, and the unwinding reaction was initiated by adding 1 mM ATP (see Experimental Procedures). (A) The kinetic time courses for the 5- and 10-nt-tailed substrates. The solid lines were three-exponential fits of the data. (B) Amplitudes of the fast and two slow phases and the total amplitude. (C) Rates of the three phases.

The amplitude of the second slow phase $A_{slow,2}$ was independent of the substrate tail length. We attribute this phase to helicase-catalyzed unwinding of the DNA substrate from the blunt end. We have observed that blunt-ended 16-bp DNA substrate can be also unwound, though much more slowly, by the helicase under the same multiple-turnover conditions (data not shown).

Kinetic Step Size in DNA Unwinding. The step size is a very useful parameter for understanding the mechanism underlying the helicase activity. Different helicases have been shown to have quite different step sizes, ranging from 1 to 9 bp, reflecting the diversity and complexity of helicases. Some examples of determined step sizes are 1.4 bp for DnaB (*28*), 3.2 bp for Dda (*29*), 3.4 bp for RecBCD (*30*), 4 bp for PcrA (*27*), 4.4 bp for UvrD (*19*), 4.5 bp for Rep (*26*), 6 bp for NPH-II (*31*), 6−8 bp for TraI (*25*), and 9.2 bp for NS3h (*32*).

To determine the step size of the BLM helicase core, we performed single-turnover unwinding experiments using 10-nt-tailed DNA substrates of different duplex lengths (12, 16,

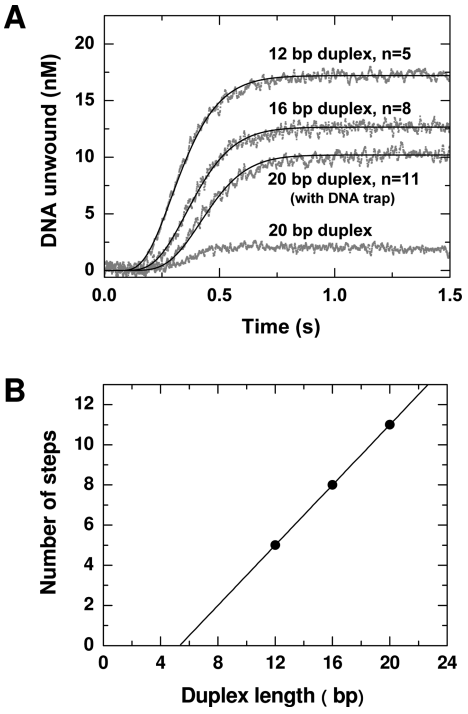

FIGURE 4: Single-turnover DNA unwinding of 10-nt-tailed ss/dsDNA of different duplex lengths. A 40 nM DNA substrate was first preincubated with 30 nM enzyme in the reaction buffer at 25 °C, and the unwinding reaction was initiated by adding 1 mM ATP and 50 μM protein trap (dT_{56}). For the 20-bp substrate, an additional measurement with 40 μM DNA trap to reduce the reannealing effect was also taken. The DNA trap was a 10-nt ssDNA that was complementary to the first 10 nucleotides (from the ss/dsDNA junction) of the top strand. It was added together with ATP and the protein trap upon unwinding initiation. (A) Kinetic time courses. The solid lines were best fits of the data to eq 3 with $n = 5$, 8, and 11 for the 12-, 16-, and 20-bp data curves, respectively. Fitted values of the amplitude (A) and unwinding rate for each step (k_{obs}) are $A = 17.2 \pm 0.1$ nM and $k_{obs} = 16.3 \pm 0.2$ s^{-1}, 12-bp substrate; $A = 12.6 \pm 0.1$ nM and $k_{obs} = 20.4 \pm 0.3$ s^{-1}, 16-bp substrate; $A = 10.2 \pm 0.1$ nM and $k_{obs} = 23.8 \pm 0.9$ s^{-1}, 20-bp substrate. (B) The number of steps as a function of duplex length. The line is a linear fit with a slope of 0.75 bp^{-1}, corresponding to a step size of ~1.33 bp.

20, 25 bp). For obtaining FRET signal changes with high signal-to-noise ratio, we used a high DNA concentration (40 nM) and a subsaturating helicase concentration (30 nM), similar to the pre-steady-state assay with a protein trap (Figure 2A). Under these conditions, each DNA substrate was, in principle, unwound at most by a single helicase monomer and in only one reaction cycle.

Typical unwinding curves are given in Figure 4A. The amplitude decreases significantly with increasing duplex length and becomes negligible at 25 bp (data not shown). Thus it appears that the helicase monomer has a high probability to dissociate from the substrate during unwinding, leading to a low processivity. This will be further studied later.

For the long duplex substrates (20 and 25 bp), there is another important reason for the exceptionally low amplitude: the two newly separated ssDNA strands are long enough to reanneal behind the single helicase monomer during the course of unwinding. This has also been observed for *E. coli* RecQ (*16*). RecQ has a high processivity, but the unwinding efficiency started to decrease for 20 bp or longer substrates due to the reannealing effect. Interestingly, this effect is obvious only when the unwinding rate of the helicase is not very high so that the two newly produced ssDNA strands have enough time to reanneal before they are totally separated. Thus it is observable only for helicases such as the NS3h helicase (~1.6 bp s^{-1} (*32*)), RecQ (~50 bp s^{-1} (*16*)), and BLM helicase core (~27 bp s^{-1}; see next). When a helicase unwinds DNA very rapidly, this reannealing effect is negligible, and the unwinding amplitude will be either independent of the duplex length, such as TraI (~1000 bp s^{-1} (*25*)) or decrease with increasing duplex length solely due to a limited processivity such as Dda (~300 bp s^{-1} (*29*)). To reduce the effect of reannealing for the 20-bp substrate, we then used a 10-nt ssDNA trap that was complementary to the first 10 nucleotides (from the ss/dsDNA junction) of the top strand. The ssDNA trap was added together with the protein trap and ATP upon unwinding initiation. As expected, the unwinding efficiency was significantly enhanced (Figure 4A).

We used eq 3 to fit the data curves for the 12- and 16-bp substrates and that for the 20-bp substrate with DNA trap. From the fittings we obtained the number of steps for the three substrates (Figure 4B). Then a linear fit of the results give a step size of ~1.33 bp. This value indicates that the BLM helicase core may unwind one base pair in a single kinetic step, similar to *E. coli* RecQ (*16*).

From the average value of the observed unwinding rate (20.2 ± 3.8 s^{-1}) and the step size, we know that the macroscopic unwinding rate of the BLM helicase core is 26.9 ± 5.1 bp s^{-1}, which is lower than that of RecQ (~50 bp s^{-1}) (*16*).

Dissociation Kinetics of BLM from DNA Substrates. For a molecular motor to move along a track, its binding sites to the track usually need to alternate between strong and weak bindings during each NTPase cycle. This modulation of binding is achieved by its nucleotide state transition. Having established that the BLM helicase core unwinds duplex DNA as monomers and with a low processivity, it is of interest to investigate in which nucleotide state the helicase tends to dissociate from the DNA substrate. For molecular motors for intracellular transport such as kinesin and myosin, the nucleotide dependences of their binding for tracks are well characterized (*33*, *34*). Though this information is very useful for understanding the mechanism of motor movement, it is still lacking for many helicases.

Here we resorted to the fluorescence polarization anisotropy assay to measure the dissociation kinetics of the bound BLM helicase core from DNA substrates under conditions of different nucleotide cofactors. The ATP state was simulated with the nonhydrolyzable ATP analogue AMPPNP and the ADP·P_i transition state with ADP·MgF_3.

We first used a fluorescein-labeled 10-nt 3′-tailed 16-bp ss/dsDNA as the substrate. This substrate was the same as that used for DNA unwinding. We observed that the dissociation from this substrate exhibited similar behaviors under conditions of different nucleotide states: occurring in two phases, a slow one and a fast one (Figure 5A). The slow phase should describe the actual dissociation process of the helicase from the ss/dsDNA junction. The fast phase, we think, should correspond to the dissociation process for helicase monomers that were bound less tightly to the end of the ssDNA tail.

For comparison, we then measured the dissociation kinetics of BLM from fluorescein-labeled 20-nt ssDNA and from 20-bp blunt-ended dsDNA substrates. For the ssDNA, the dissociation also occurred in a slow phase and a fast phase as for ss/dsDNA. Similarly, the slow phase describes the actual dissociation process, and the fast one is attributed to helicase monomers bound less tightly to the ends of the ssDNA. For the blunt-ended dsDNA, only one rapid phase was observed in all nucleotide

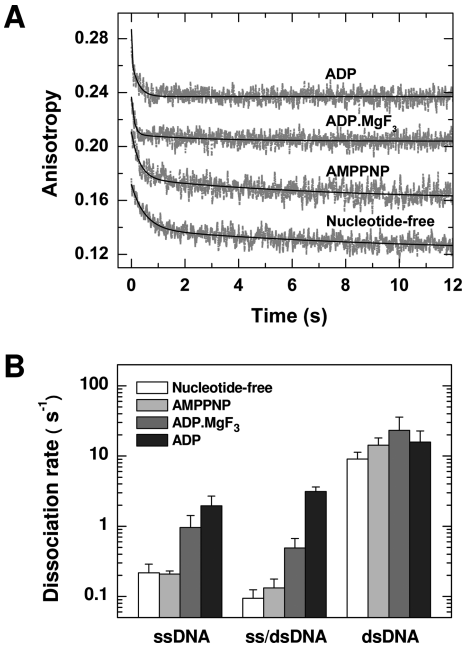

FIGURE 5: Dissociation kinetics of bound helicase from DNA substrates in the presence or absence of nucleotide cofactors. 40 nM DNA substrate was preincubated with 200 nM enzyme in the reaction buffer at 25 °C for 5 min, and the reaction was initiated by adding 2 μM protein trap (dT_{56}) without or with 1 mM nucleotide cofactors (AMPPNP or ADP) as indicated. In the case of ADP·MgF_3, 1 mM NaF was added during the preincubation of DNA and helicase (see Experimental Procedures). (A) Kinetic time courses for a 10-nt 16-bp ss/dsDNA substrate. The curves of AMPPNP, ADP·MgF_3, and ADP were displaced vertically for clarity. The solid lines were double-exponential fits of the data, with dissociation rates summarized in Table 2. (B) Dissociation rates for the helicase from different DNA substrates (20-nt ssDNA, 10-nt 16-bp ss/dsDNA, and 20-bp blunt-ended dsDNA). In the cases of the biphasic dissociation process, only the relevant slow-phase rates were shown.

Table 2: Dissociation Rates for the Helicase from DNA Substrates in Different Nucleotide States

	ssDNA		ss/dsDNA		dsDNA
nucleotide state	k_1 (s^{-1})	k_2 (s^{-1})	k_1 (s^{-1})	k_2 (s^{-1})	k (s^{-1})
nucleotide free	0.22 ± 0.07	1.3 ± 0.5	0.09 ± 0.03	2.0 ± 0.5	9.1 ± 2.2
AMPPNP	0.21 ± 0.02	2.1 ± 0.2	0.13 ± 0.05	3.3 ± 0.7	14.3 ± 3.9
ADP·MgF_3	0.96 ± 0.46	16.9 ± 7.2	0.49 ± 0.18	9.6 ± 1.9	23.3 ± 12.6
ADP	1.96 ± 0.72	47.6 ± 22.7	3.12 ± 0.51	43.5 ± 17.3	15.8 ± 7.0

states. All of the dissociation rates obtained from data fittings of the kinetic curves are summarized in Table 2. The corresponding fractions of total anisotropy signal change associated with the two rates are given in Table S2 in the Supporting Information. The similar fast-phase rates for ssDNA and ss/dsDNA substrates in a given nucleotide state support our idea about the origin of the fast phase.

For clarity, we have presented in Figure 5B the relevant dissociation rates under all of the different conditions. From these data we may notice several obvious features. (a) The helicase binds to the ss- and ss/dsDNA substrates more tightly in nucleotide-free and ATP states than in the ADP·P_i and ADP states. (b) The helicase binds weakly to the dsDNA substrate in all nucleotide states. (c) The helicase binds more tightly to the ss/dsDNA substrates than the ss- and dsDNA substrates in almost all nucleotide states, implying that the helicase bound at a ss/dsDNA junction interacts with the ss- and dsDNA regions of the substrate simultaneously.

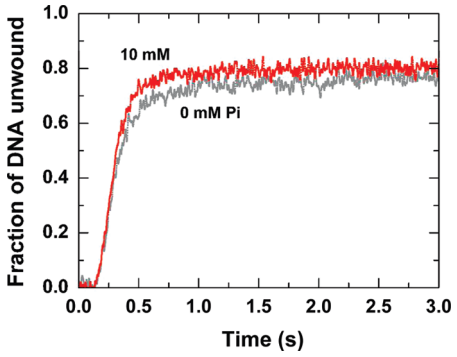

FIGURE 6: Single-turnover DNA unwinding in the absence or presence of 10 mM P_i. A 5 nM 10-nt-tailed 12-bp ss/dsDNA substrate was first preincubated with 40 nM enzyme in the reaction buffer at 25 °C, and the unwinding reaction was initiated by adding ATP (1 mM), protein trap (dT_{56}, 3 μM), and P_i (0 or 10 mM).

From the results with ss/dsDNA, it appears that the low processivity of the helicase should result from its relatively high dissociation rates (~0.5 and 3 s^{-1}) in the ADP·P_i and ADP states during its ATPase cycle. The probability of dissociation in the other two states should be negligible due to the much lower dissociation rates (~0.1 s^{-1}).

Inhibition of the Helicase Activity by ADP. To verify the above results, we studied the inhibiting effect of P_i and ADP on the helicase activity of the enzyme. The experiments were performed under single-turnover conditions while adding P_i or ADP to the reaction buffer. In the presence of P_i, the lifetime of the weak DNA-binding ADP·P_i state should be extended in each ATPase cycle (or unwinding step). Thus we expect that the DNA unwinding efficiency should be somewhat decreased due to enhanced dissociation probability. But we have observed that even 10 mM P_i did not affect much either the unwinding amplitude or unwinding rate (Figure 6), suggesting that P_i release is a very rapid substep in the ATPase cycle of the helicase.

In the presence of ADP, however, the helicase activity was indeed inhibited seriously (Figure 7). At 2 mM ADP, the unwinding amplitude became as low as ~10%. The unwinding rate also decreased with increasing [ADP], though not as significantly as the amplitude. Thus, in the presence of ADP, the lifetime of the weak DNA-binding ADP state is extended, resulting in an increased dissociation probability of the helicase from the substrate and a prolonged ATPase cycle during DNA unwinding.

According to the above dissociation and inhibition results, the kinetic mechanism for DNA unwinding of the BLM helicase core in one ATPase cycle is proposed and outlined in Scheme 1, where ES represents the enzyme−substrate complex in the nucleotide-free state. k_d is the rate constant for enzyme dissociation from the DNA substrate in the ADP state; dissociation in the other states is neglected.

From Scheme 1 and assuming the dissociation probability of the helicase in each ATPase cycle was not high, approximate expressions for the processivity P and the unwinding rate for each step k_{obs} in the presence of [ADP] can be derived:

$$P = \frac{k_3}{k_3 + k_d} - \frac{k_d(k_{-1} + k_2)k_{-3}[\mathrm{ADP}]}{k_1 k_2 (k_3 + k_d)\ [\mathrm{ATP}]} \quad (4)$$

$$k_{obs} = \left(\frac{1}{k_{obs}^{(0)}} + \frac{(k_{-1} + k_2)k_{-3}[\mathrm{ADP}]}{k_1 k_2 (k_3 + k_d)\ [\mathrm{ATP}]} \right)^{-1} \quad (5)$$

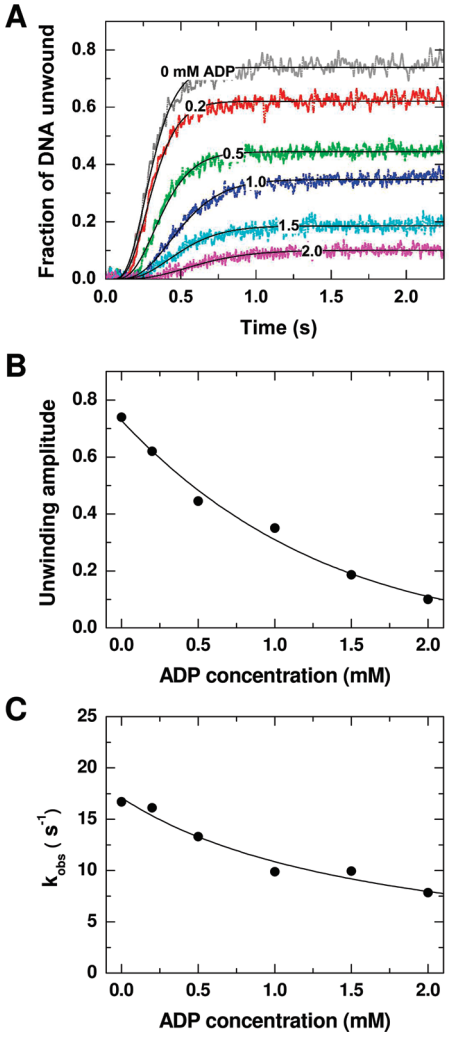

FIGURE 7: Single-turnover DNA unwinding in the presence of ADP. The measurements were carried out under the same conditions as in Figure 6, except that P_i was replaced with ADP (concentrations indicated). (A) Kinetic time courses. The solid lines were best fits of the data to eq 3 with $n = 5$. (B) Unwinding amplitude. The line corresponded to a best fit of the data to the equation $A = (1 - x)P^5$, where x is the fraction of BLM that dissociates from the substrate before unwinding occurs, P is the processivity as given by eq 4, and integer 5 is the number of unwinding steps for the 12-bp substrate (Figure 4). Assuming $x = 0$, the fitted values are $k_3/(k_3 + k_d) = 0.94 \pm 0.01$ and $k_d(k_{-1} + k_2)k_{-3}[k_1k_2(k_3 + k_d)]^{-1} = 0.15 \pm 0.01$. (C) The observed rate for each unwinding step. The line was a best fit of the data to eq 5. The fitted values are $k_{obs}^{(0)} = 17.2 \pm 0.6\ s^{-1}$ and $(k_{-1} + k_2)k_{-3}[k_1k_2(k_3 + k_d)]^{-1} = 0.033 \pm 0.004$ s.

with

$$k_2 \equiv \left(\frac{1}{k_2'} + \frac{1}{k_2''}\right)^{-1} \tag{6}$$

$$k_{obs}^{(0)} = \left(\frac{1}{k_1[\mathrm{ATP}]} + \frac{k_{-1}}{k_1[\mathrm{ATP}]k_2} + \frac{1}{k_2} + \frac{1}{k_3 + k_d}\right)^{-1} \tag{7}$$

where the processivity P is defined as the probability of completing one round of ATP binding and hydrolysis and $k_{obs}^{(0)}$ is the unwinding rate for each step in the absence of ADP.

With eq 4, the data in Figure 7B can be fitted. Neglecting the possible dissociation of bound helicase from the substrate before unwinding initiation, we obtained $k_3/(k_3 + k_d) = 0.94 \pm 0.01$, which is the processivity in the absence of ADP, and

Scheme 1

$k_d(k_{-1} + k_2)k_{-3}[k_1k_2(k_3 + k_d)]^{-1} = 0.15 \pm 0.01$. In combination with the short step size (1 bp), the processivity of 0.94 can affect significantly the unwinding efficiency of long substrates (see Discussion).

Similarly, the data in Figure 7C can be fitted with eq 5, giving $k_{obs}^{(0)} = 17.2 \pm 0.6\ s^{-1}$ and $(k_{-1} + k_2)k_{-3}[k_1k_2(k_3 + k_d)]^{-1} = 0.033 \pm 0.004$ s. From the fitted values of $k_d(k_{-1} + k_2)k_{-3}[k_1k_2(k_3 + k_d)]^{-1}$ and $(k_{-1} + k_2)k_{-3}[k_1k_2(k_3 + k_d)]^{-1}$ we obtain the dissociation rate for the BLM helicase core in ADP state as $k_d = 0.15/0.033 = 4.5\ s^{-1}$. This value is in agreement with that obtained from direct measurement ($3.12 \pm 0.51\ s^{-1}$; Figure 5 and Table 2).

Modulation by DNA of the Binding Affinity for ATP and ADP. From the above studies, it is clear that the inhibition of the helicase activity by ADP is mainly due to the competitive binding of ADP to the ATP-binding site of the helicase, thus effectively extending the lifetime of the ADP state. Here we used fluorometric titration assays to study more directly ATP and ADP bindings to the helicase and their modulation by DNA substrate.

We first titrated a 0.2 μM helicase solution with a fluorescent analogue of ATP, mantATP, in the absence of ADP and DNA. We see that mantATP binds to the BLM helicase core with a high affinity (Figure 8A). The apparent dissociation constant was determined as $K_d^{ATP} = 30.8 \pm 2.9$ nM. Next we studied the effect of ADP on ATP binding in the absence of DNA. Helicase (0.2 μM) and 5 μM mantATP were preincubated for 5 min in the reaction buffer. Then the solution was titrated with ADP, and the fluorescence of mantATP was monitored. As shown in Figure 8B, the fluorescence signal decreased significantly with increasing ADP concentration, indicating that ADP may displace effectively the bound mantATP molecules and bind tightly to the helicase.

In this assay, the fluorescence of mantATP is described by eq 8

$$F = F_s + f_d[\mathrm{mantATP}] + (f_c - f_d)[\mathrm{E{\cdot}mantATP}] \tag{8}$$

where [E·mantATP] is the concentration of the helicase in complex with mantATP. Under the present experimental conditions where the mantATP concentration was much higher than that of the helicase as well as than K_d^{ATP}, the expression for [E·mantATP] can be easily derived as

$$[\mathrm{E{\cdot}mantATP}] = \frac{(K_d^{ADP}/K_d^{ATP})[\mathrm{mantATP}]}{(K_d^{ADP}/K_d^{ATP})[\mathrm{mantATP}] + K_d^{ADP} + [\mathrm{ADP}]}[E_T] \tag{9}$$

where K_d^{ADP} is the apparent dissociation constant for ADP and $[E_T]$ is the total helicase concentration.

Fitting the data in Figure 8B with eq 8 gave (K_d^{ADP}/K_d^{ATP})-[mantATP] + $K_d^{ATP} = 21.8 \pm 0.6$ μM. From this value together with $K_d^{ADP} = 30.8 \pm 2.9$ nM and [mantATP] = 5 μM, we obtained $K_d^{ADP} = 135 \pm 17$ nM.

It is well-known that the ATPase activity of a helicase usually is significantly stimulated by DNA substrate. Therefore, we repeated the above experiments while using saturating 10-nt 16-bp

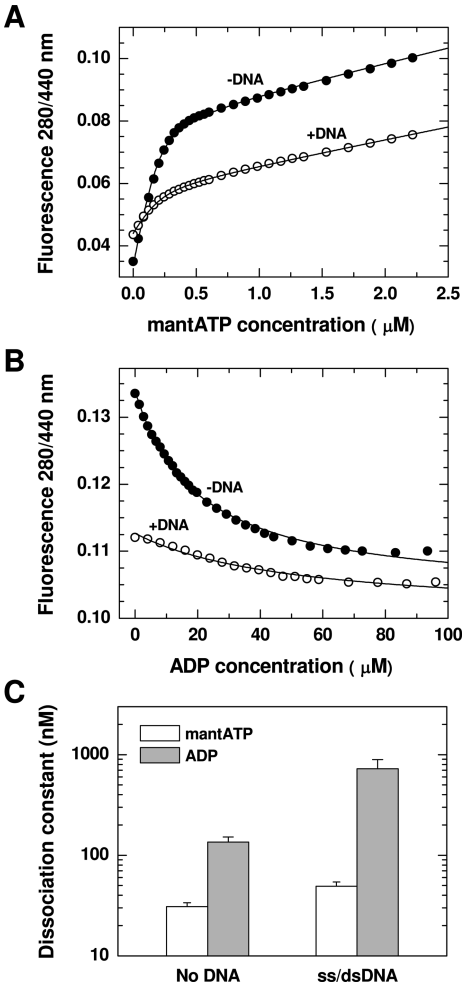

FIGURE 8: Equilibrium ATP and ADP binding to the BLM helicase core. (A) Fluorometric mantATP-binding assay. A 1 mL solution of 0.2 μM enzyme with or without 2 μM 10-nt 16-bp ss/dsDNA in the reaction buffer was titrated with mantATP (see Experimental Procedures). The fluorescence of mantATP was corrected for the inner filter effect and dilution effect. The lines represent the best fits of the data to eq 2, giving $K_d^{ATP} = 30.8 \pm 2.9$ (−DNA) or 49.3 ± 5.0 nM (+DNA). (B) Competitive binding of ATP and ADP to BLM. 0.2 μM enzyme with or without 2 μM ss/dsDNA was first preincubated with 5 μM mantATP in 1 mL of reaction buffer for 5 min. Then the solution was titrated with ADP. The fluorescence of mantATP was corrected for the inner filter effect and dilution effect. The lines were best fits of the data to eq 8, giving $(K_d^{ADP}/K_d^{ATP})[\text{mantATP}] + K_d^{ADP} = 21.8 \pm 0.6$ (−DNA) or 73.3 ± 9.7 μM (+DNA). (C) Dissociation constants for ATP and ADP in the absence and presence of DNA.

ss/dsDNA. The experimental results are also given in Figure 8A, B, which are indeed different from the corresponding ones without DNA. From the results we obtained in the presence of ss/dsDNA, $K_d^{ATP} = 49.3 \pm 5.0$ nM and $K_d^{ADP} = 723 \pm 168$ nM.

For clarity, the obtained dissociation constants are presented in Figure 8C. From the values of K_d^{ATP} and K_d^{ADP} without or with DNA substrate, we know that one of the stimulating effects of DNA on the ATPase activity of the helicase is to reduce its affinity for ADP (by ~5 times) and thus enhance the ADP release rate, whereas the affinity for ATP is not modulated much by DNA. The ratio between K_d^{ADP} and K_d^{ATP} is also significantly increased (from 4.38 to 14.66) by DNA.

Assuming ADP association is diffusion-controlled ($\sim 1 \times 10^8$ M^{-1} s^{-1}), then the dissociation rate for ADP in the presence of DNA would be around 70 s^{-1}, which is much higher than the observed unwinding rate of the helicase, ~20 steps per second, and thus is not rate-limiting. In the absence of DNA, however, the dissociation rate for ADP would be reduced to ~13.5 s^{-1}. This explains, at least partially, why the ATPase activity of the helicase is much reduced without the stimulation of DNA (data not shown). The present results on the modulation of binding affinity for ATP and ADP by DNA clearly indicate that the ATP- and DNA-binding sites are coupled in the helicase.

DISCUSSION

BLM Helicase Core Catalyzes DNA Unwinding in the Monomeric Form under All Conditions Studied. Pre-steady-state kinetic measurements are sensitive for analyzing the first reaction cycle of DNA unwinding. In our assays, we have used a substrate of 10-nt tail length and enzyme concentrations lower than that of the substrate. Thus DNA binding of BLM in the monomeric form was favored. The efficient unwinding of the substrate and the linear increase of the burst amplitude with increasing enzyme concentration (Figure 2) clearly indicate that the helicase monomers are the active species in the DNA unwinding reaction. If the active form of the helicase is the oligomer, the unwinding of DNA should be negligibly low or unobservable as in the cases of dimeric Rep (*26*), UvrD (*20*), and PcrA (*27*).

In the pre-steady-state assay, both substrate tail length and enzyme concentration did not allow oligomerization of the BLM helicase core even if it was inclined to do so. In the multiple-turnover kinetic assays, however, DNA substrates of various ssDNA tail lengths have been used, and in addition, the enzyme concentration was saturating. Even under these conditions favoring oligomerization, the experimental results (Figure 3) still indicate that the helicase monomers are the active species in DNA unwinding. In the multiple-turnover assays, the fast phase was contributed by the helicase monomers that were bound to the ss/dsDNA junctions and thus was essentially independent of the tail length, in contrast with dimeric helicases such as PcrA and UvrD where the amplitude of the fast phase (or total amplitude in the case of single-turnover measurements) dramatically decreases when the ssDNA tail length is shorter than 15 bp (*27*, *35*, *36*).

Note that we attributed the first slow phase in the multiple-turnover kinetic curves to DNA unwinding by helicase molecules bound to positions away from ss/dsDNA junctions on the ssDNA tails. As the number of helicase monomers bound to the tails is proportional to the tail length, the amplitude of the first slow phase $A_{slow,1}$ accordingly depends on the tail length. In addition, as these bound monomers need first to translocate along the ssDNA tails toward the ss/dsDNA junctions before starting to unwind the duplex, the rate of this slow phase $k_{slow,1}$ should decrease with increasing tail length. But in our results (Figure 3C), $k_{slow,1}$ is approximately constant (except for the 5-nt substrate). This implies that the ssDNA translocation time of the helicase is negligible compared with other slow processes such as helicase binding to DNA.

In Figure 3, one may easily notice that the amplitude of the fast phase for the 5-nt-tailed substrate was similar to that for the other substrates while the corresponding rate was much lower. From the binding site size of a BLM monomer (~8 nt, Figure 1), it is easily expected that the binding affinity of the helicase may be lower for the 5-nt-tailed substrate than the other substrates. Therefore, the BLM monomers at the ss/dsDNA junctions of the 5-nt-tailed substrates might have a higher probability to dissociate rather than catalyze duplex unwinding upon addition of ATP. But as free helicase monomers in the solution would continuously

and rapidly bind to the vacated ss/dsDNA junctions during the whole unwinding reaction, the amplitude of the fast phase, which was contributed by both prebound and newly bound helicase monomers, was not reduced for the 5-nt-tailed substrate. The corresponding rate, on the other hand, was significantly decreased due to the repetitive binding/dissociation processes.

To verify the above proposal, we carried out single-turnover kinetic assays with 5-nt- and 10-nt-tailed substrates, where a protein trap (8 μM dT_{56}) was added together with ATP when initiating the unwinding while all of the other conditions were the same as in the multiple-turnover kinetic assays (Figure 3). In this case, the binding of helicase monomers to the DNA substrates during the course of unwinding was eliminated, and we would mainly observe DNA unwinding catalyzed by prebound helicase monomers. As expected, we observed that the unwinding amplitude for the 5-nt-tailed substrate was only about one-third of that for the 10-nt-tailed substrate, implying a much higher dissociation probability for the prebound monomers from the 5-nt-tailed than the 10-nt-tailed substrates upon unwinding initiation, whereas the unwinding rates were comparable for the two substrates (see Figure S3 in the Supporting Information).

Taken together, the experimental results from the present kinetic studies suggest that the BLM helicase core catalyzes DNA unwinding as monomers under different conditions. The observation is consistent with our previous identification of the arginine finger for ATP hydrolysis and energy coupling that is located at the interface between two domains of the BLM helicase core (*37*). Therefore, the ATPase and helicase activities of the BLM helicase core may not need its oligomerization. This is in contrast with hexameric helicases such as bacteriophage T7 gene 4 (*38*, *39*) and bovine papillomavirus E1 (*40*) where the arginine finger is located at the interface between two adjacent subunits, and thus an oligomerization is absolutely required for their ATPase and helicase activities.

Low Processivity of BLM. For molecular motors moving along a track, their binding affinity for the track is usually modulated by their nucleotide state. Accordingly, they usually have a limited processivity. Different motors, in isolation or in the presence of other accessory proteins, may be tuned to have quite different processivities so that they can carry out the allocated specific *in vivo* tasks appropriately. As long as isolated helicases are concerned, the processivity P may be as low as 0.27 (PcrA (*27*)) or as high as 0.99997 (RecBCD (*41*)). Considering the respective step sizes, the above values correspond respectively to 5.5-bp and 30-kbp duplex DNA unwound in a single binding event, the difference of which is really tremendous.

For the BLM helicase core, we observed a low processivity of $P = 0.94 \pm 0.01$ (Figure 7) or equivalently $P/(1 - P) \times$ step size = 16 ± 3 bp. This low processivity explains why the ratio between the burst amplitude and the enzyme concentration in the pre-steady-state experiments is as low as 0.58 ± 0.02 rather than close to 1 (Figure 2C). From $P = 0.94 \pm 0.01$ and the number of unwinding steps for the 12-bp duplex (i.e., 5) obtained in Figure 4, we know that the probability for a BLM monomer to finish unwinding the whole 12-bp substrate is $P^5 = 0.73 \pm 0.04$. This predicted value is not far from the obtained ratio of 0.58 ± 0.02. Therefore, we may be certain that the three other possible factors proposed previously for the low ratio, i.e., (i) not all enzyme molecules bound to the substrates, (ii) some enzyme molecules dissociated from the substrates upon unwinding initiation, and (iii) some enzyme molecules bound to the blunt ends rather than ss/dsDNA junctions of the substrates, could not be significant and lead to, at most, an ~15% reduction in the unwinding efficiency.

It is worth mentioning that *E. coli* RecQ was shown to have a much higher affinity for the ss/dsDNA junction than blunt-ended dsDNA (*16*). From the conclusions just mentioned above, it seems that the BLM helicase has DNA-binding properties similar to those of RecQ. To verify this, we carried out two unwinding experiments. One was performed under the same conditions as in Figure 2B (60 nM ss/dsDNA, 40 nM BLM); the other was performed also under the same conditions except that 60 nM 12-bp blunt-ended dsDNA (with no fluorophores) was added in the preincubation solution for ss/dsDNA and BLM. As shown in Figure S4 in the Supporting Information, the addition of blunt-ended dsDNA only reduced slightly the DNA unwinding efficiency. This implies that, under the subsaturating conditions, most helicase molecules still bound to the ss/dsDNA even in the presence of blunt-ended dsDNA. That is, the BLM helicase prefers binding to ss/dsDNA junctions rather than blunt ends of dsDNA.

Our dissociation kinetics and helicase activity inhibition experiments (Figures 5 and 7) unambiguously indicate that this low processivity is mainly caused by the high substrate release rate of BLM in the ADP state during its ATPase cycle for DNA unwinding. For the DExH RNA helicase NPH-II, it has been previously shown by RNA unwinding measurements that it may dissociate from the RNA substrate in "non-ATP-bound" states (i.e., ADP·P_i, ADP, or nucleotide free) (*31*). By carrying out similar inhibition studies, it would be easy to find out the definite nucleotide state of weak substrate binding for the helicase.

At present, only a relatively limited number of helicases have their nucleotide-dependent DNA-binding affinities well characterized. From these data, it is clear that there is no common mode for the control of the substrate affinity by nucleotide cofactors. For example, for PriA (*42*), Rep (*43*), and NS3h (*18*), the ATP state is the relatively weak ssDNA-binding state. For DnaB (*44*) and bacteriophage T7 helicase (*45*), the nucleotide-free state is the weak ssDNA-binding state. These differences imply that, from helicase to helicase, the operation mechanism of substrate unwinding may be more diversified than expected at the molecular level.

Implications for the Mechanism of DNA Unwinding by BLM. Various models have been proposed to explain the DNA (or RNA) unwinding activities of different helicases. For monomeric helicases, there are two prevailing mechanisms that can well describe stepping motion of the helicase along the DNA substrate: inchworm model (*46*, *47*) and Brownian motor model (*48*). In the inchworm model, the helicase binds to the ssDNA with two binding sites which, through coupling with nucleotide-state transition during an ATPase cycle, alternate between strong and weak interactions with DNA and move relative to each other, thus resulting in directional ssDNA translocation and duplex unwinding. In the Brownian motor model as proposed for HCV, the helicase has simply a single DNA-binding site modulated by nucleotide state: ssDNA-binding energy fuels the opening of dsDNA and directional stepping, while the random motion in the weak DNA-binding period adjusts the helicase position for the next cycle (*48*).

Crystal structures of the superfamily 1 helicases PcrA (*47*) and UvrD (*49*) in complex with ss/dsDNA substrate and different nucleotides support the inchworm model. In these structures, ssDNA binds to the top of two RecA-like domains (1A and 2A) with interactions modulated by the nucleotide state, and the cleft

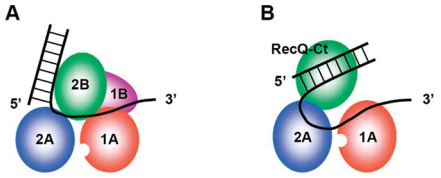

FIGURE 9: (A) Schematic illustration of the ss/dsDNA-binding mode for SF1 helicases such as PcrA and UvrD as determined from crystal structures (*47*, *49*). 1A and 2A are the two RecA-like domains, and the ATP-binding site between the two domains is indicated. (B) Proposed ss/dsDNA-binding mode for RecQ (*52*, *53*) and BLM (*6*).

between the two domains, where ATP binding and hydrolysis occur, may be opened or closed depending on the nucleotide state (Figure 9A). An ssDNA translocation step size of 1 nt determined for both PcrA (*50*) and UvrD (*51*) is consistent with the inchworm model.

Crystal structures of the BLM helicase core, in complex with DNA substrate or alone, are still unavailable. Fortunately, the structure of a major part of one of its homologues, the catalytic core of *E. coli* RecQ, has been well resolved in the absence of DNA (*52*), which is composed of two RecA-like domains and a RecQ-conserved (RecQ-Ct) domain. The latter is further divided into two subdomains. Based on the structural and mutational studies, a model for ss/dsDNA binding of RecQ has been proposed (*52*, *53*), in which the 3′ ssDNA tail of the substrate binds across the front surfaces of the two RecA-like domains and the dsDNA to be unwound binds to the RecQ-Ct domain (Figure 9B).

Previously, we have modeled the structure of the BLM helicase core by homology modeling using both amino acid sequence alignment and the template structure of RecQ (*6*). We found that most of the disease-linked mutations of BLM are located at or near the ATP- and DNA-binding sites in the modeled structure. Thus we believe the BLM helicase core uses very probably the same mode for ss/dsDNA binding as that proposed for RecQ.

From the proposed ss/dsDNA model for BLM (Figure 9B), it is still not very clear as to how the helicase makes stepping motion and unwinds DNA duplex. But as discussed below, results from our present study imply that the BLM helicase core may unwind duplex DNA in an inchworm manner.

(a) The kinetic step size determined for BLM is 1 bp (Figure 4). Although a kinetic step size corresponds to the average number of bases translocated or base pairs unwound between two successive rate limiting steps and is not always the same as the mechanical step size related to one ATP hydrolyzed (*51*), our result suggests that the BLM helicase core very probably unwinds dsDNA with a mechanical step determined by the 1-nt ssDNA translocation step predicated by an inchworm mechanism.

(b) From the dissociation measurements (Figure 5), we know that the binding affinity of BLM for ss- and ss/dsDNA substrates is modulated by the nucleotide state. This is consistent with the requirements for a helicase to translocate along ssDNA and unwind dsDNA with the inchworm mechanism. Note that the quick dissociation from ss/dsDNA in the ADP state indicates that the helicase has a relatively weak DNA-binding affinity, which seems to support that BLM may unwind dsDNA as a Brownian motor like HCV helicase (*48*). But actually, the DNA-binding affinity in the ADP state could not be much lower than that in the other states because, according to the Arrhenius relation, a 10-fold difference in dissociation rate only means a binding energy difference of 2.3 k_BT. Furthermore, the affinity for ADP binding is significantly modulated by DNA (Figure 8C), implying that the helicase in the ADP state still interacts effectively with DNA.

According to crystal structures of PcrA, UvrD, and Rep (*47*, *49*, *54*), the cleft between the two RecA-like domains in the presence of DNA is opened in the apo state, closed from ATP binding to hydrolysis (ADP·P_i state), and reopened again in the ADP state. Therefore, if BLM indeed uses an inchworm mechanism to make stepping motion like PcrA, UvrD, and Rep, a forward step in each ATPase cycle should be taken when the 1A domain binds to ssDNA tightly and the 2A domain loosens ssDNA and moves away from the 1A domain upon P_i release. This requires that ssDNA binding for the helicase in the ADP state relies mainly on the 1A domain. In other words, it is only in the ADP state that the helicase binds the ssDNA without utilizing the 2A domain. The dissociation result that DNA binding is the weakest in the ADP state for BLM seems to be consistent with such a scenario. Note that the interdomain cleft is still opened in the ATP state in the structure of RecQ (*52*). We think this is possibly because of the lack of DNA to trigger the cleft closing. Single-molecule FRET experiments with the *Bacillus subtilis* YxiN helicase clearly show that only cooperative binding of both RNA and ATP induces a closure of the interdomain cleft (*55*).

(c) The helicase binds relatively weakly to the dsDNA substrate in all nucleotide states (Figure 5). This is logical if BLM uses an inchworm mechanism in DNA unwinding. As can be seen in Figure 9B, a strong dsDNA binding would impede the forward movement of the helicase along the ssDNA tail. A too weak or no dsDNA binding, on the other hand, would make it difficult for the helicase to disrupt the hydrogen bonds and displace the opposite DNA strand simply by ssDNA translocation alone because the ssDNA binds only to the surfaces of domains 1A and 2A. This is different from such cases as hexameric (*40*, *56*) or monomeric helicases (*57*) where the translocated ssDNA is deeply wrapped inside the enzyme, and thus ssDNA translocation alone could accomplish displacement of the opposite strand and duplex separation without needing the dsDNA to be well oriented or fixed by specific interaction with the helicase.

In summary, we have characterized the DNA unwinding behaviors of the helicase core of the BLM protein under various conditions and provided evidence that suggests that the BLM helicase core always functions as monomers. The low value of its step size indicates that BLM unwinds only one base pair in a single kinetic step. If this is also the mechanical step size, then the mechanochemical coupling efficiency would seem to be low. But the RecQ family helicases mainly function at the interface of DNA replication, recombination, and repair to maintain genomic integrity by resolving, in addition to unwinding the standard B-form DNA duplex, secondary DNA structures such as the G-quadruplex DNA, D-loops, and Holliday junction (*3*, *9*). Therefore, it is reasonable to believe that the helicase activities of these enzymes are more efficiently "tuned" for unwinding the specific DNA structures.

The experimental results in the present study imply that the BLM helicase core probably translocates along ssDNA and unwinds dsDNA using an inchworm mechanism. Further studies on the nucleotide-state-modulated interactions between the helicase and DNA as well as the mechanical movement of the two RecA-like domains are necessary for defining an accurate DNA unwinding mechanism for BLM. Crystal structures of the helicase in complex with ss/dsDNA and different nucleotides would certainly provide more direct and important information.

SUPPORTING INFORMATION AVAILABLE

Four figures and two tables as described in the text. This material is available free of charge via the Internet at http://pubs.acs.org.

REFERENCES

1. German, J. (1997) Bloom's syndrome. XX. The first 100 cancers. *Cancer Genet. Cytogenet. 93*, 100–106.
2. Chaganti, R. S., Schonberg, S., and German, J. (1974) A manyfold increase in sister chromatid exchanges in Bloom's syndrome lymphocytes. *Proc. Natl. Acad. Sci. U.S.A. 71*, 4508–4512.
3. Hickson, I. D. (2003) RecQ helicases: caretakers of the genome. *Nat. Rev. Cancer 3*, 169–178.
4. Ellis, N. A., Groden, J., Ye, T. Z., Straughen, J., Lennon, D. J., Ciocci, S., Proytcheva, M., and German, J. (1995) The Bloom's syndrome gene product is homologous to RecQ helicases. *Cell 83*, 655–666.
5. Guo, R. B., Rigolet, P., Zargarian, L., Fermandjian, S., and Xi, X. G. (2005) Structural and functional characterizations reveal the importance of a zinc binding domain in Bloom's syndrome helicase. *Nucleic Acids Res. 33*, 3109–3124.
6. Guo, R.-B., Rigolet, P., Ren, H., Zhang, B., Zhang, X.-D., Dou, S.-X., Wang, P.-Y., Amor-Gueret, M., and Xi, X. G. (2007) Structural and functional analyses of disease-causing missense mutations in Bloom syndrome protein. *Nucleic Acids Res. 35*, 6297–6310.
7. Liu, J. L., Rigolet, P., Dou, S.-X., Wang, P.-Y., and Xi, X. G. (2004) The zinc finger motif of *Escherichia coli* RecQ is implicated in both DNA binding and protein folding. *J. Biol. Chem. 279*, 42794–42802.
8. Janscak, P., Garcia, P. L., Hamburger, F., Makuta, Y., Shiraishi, K., Imai, Y., Ikeda, H., and Bickle, T. A. (2003) Characterization and mutational analysis of the RecQ core of the bloom syndrome protein. *J. Mol. Biol. 330*, 29–42.
9. Bennett, R. J., and Keck, J. L. (2004) Structure and function of RecQ DNA helicases. *Crit. Rev. Biochem. Mol. Biol. 39*, 79–97.
10. Karow, J. K., Constantinou, A., Li, J. L., West, S. C., and Hickson, I. D. (2000) The Bloom's syndrome gene product promotes branch migration of holliday junctions. *Proc. Natl. Acad. Sci. U.S.A. 97*, 6504–6508.
11. Wu, L., and Hickson, I. D. (2003) The Bloom's syndrome helicase suppresses crossing over during homologous recombination. *Nature 426*, 870–874.
12. Wu, L., Bachrati, C. Z., Ou, J., Xu, C., Yin, J., Chang, M., Wang, W., Li, L., Brown, G. W., and Hickson, I. D. (2006) BLAP75/RMI1 promotes the BLM-dependent dissolution of homologous recombination intermediates. *Proc. Natl. Acad. Sci. U.S.A. 103*, 4068–4073.
13. Karow, J. K., Newman, R. H., Freemont, P. S., and Hickson, I. D. (1999) Oligomeric ring structure of the Bloom's syndrome helicase. *Curr. Biol. 9*, 597–600.
14. Singleton, M. R., Dillingham, M. S., and Wigley, D. B. (2007) Structure and mechanism of helicases and nucleic acid translocases. *Annu. Rev. Biochem. 76*, 23–50.
15. Lohman, T. M., Tomko, E. J., and Wu, C. G. (2008) Non-hexameric DNA helicases and translocases: mechanisms and regulation. *Nat. Rev. Mol. Cell. Biol. 9*, 391–401.
16. Zhang, X.-D., Dou, S.-X., Xie, P., Hu, J. S., Wang, P.-Y., and Xi, X. G. (2006) *Escherichia coli* RecQ is a rapid, efficient, and monomeric helicase. *J. Biol. Chem. 281*, 12655–12663.
17. Xu, H. Q., Zhang, A. H., Auclair, C., and Xi, X. G. (2003) Simultaneously monitoring DNA binding and helicase-catalyzed DNA unwinding by fluorescence polarization. *Nucleic Acids Res. 31*, e70.
18. Levin, M. K., Gurjar, M. M., and Patel, S. S. (2003) ATP binding modulates the nucleic acid affinity of hepatitis C virus helicase. *J. Biol. Chem. 278*, 23311–23316.
19. Ali, J. A., and Lohman, T. M. (1997) Kinetic measurement of the step size of DNA unwinding by *Escherichia coli* UvrD helicase. *Science 275*, 377–380.
20. Ali, J. A., Maluf, N. K., and Lohman, T. M. (1999) An oligomeric form of *E. coli* UvrD is required for optimal helicase activity. *J. Mol. Biol. 293*, 815–834.
21. Umezu, K., Nakayama, K., and Nakayama, H. (1990) *Escherichia coli* RecQ protein is a DNA helicase. *Proc. Natl. Acad. Sci. U.S.A. 87*, 5363–5367.
22. Karow, J. K., Chakraverty, R. K., and Hickson, I. D. (1997) The Bloom's syndrome gene product is a 3′-5′ DNA helicase. *J. Biol. Chem. 272*, 30611–30614.
23. Nanduri, B., Byrd, A. K., Eoff, R. L., Tackett, A. J., and Raney, K. D. (2002) Pre-steady-state DNA unwinding by bacteriophage T4 Dda helicase reveals a monomeric molecular motor. *Proc. Natl. Acad. Sci. U.S.A. 99*, 14722–14727.
24. Liao, J.-C., Jeong, Y.-J., Kim, D.-E., Patel, S. S., and Oster, G. (2005) Mechanochemistry of T7 DNA helicase. *J. Mol. Biol. 350*, 452–475.
25. Sikora, B., Eoff, R. L., Matson, S. W., and Raney, K. D. (2006) DNA unwinding by *Escherichia* coli DNA helicase I (TraI) provides evidence for a processive monomeric molecular motor. *J. Biol. Chem. 281*, 36110–36116.
26. Cheng, W., Hsieh, J., Brendza, K. M., and Lohman, T. M. (2001) *E. coli* Rep oligomers are required to initiate DNA unwinding *in vitro*. *J. Mol. Biol. 310*, 327–350.
27. Yang, Y., Dou, S.-X., Ren, H., Wang, P.-Y., Zhang, X.-D., Qian, M., Pan, B.-Y., and Xi, X. G. (2008) Evidence for a functional dimeric form of the PcrA helicase in DNA unwinding. *Nucleic Acids Res. 36*, 1976–1989.
28. Galletto, R., Jezewska, M. J., and Bujalowski, W. (2004) Unzipping mechanism of the double-stranded DNA unwinding by a hexameric helicase: quantitative analysis of the rate of the dsDNA unwinding, processivity and kinetic step-size of the *Escherichia coli* DnaB helicase using rapid quench-flow method. *J. Mol. Biol. 343*, 83–99.
29. Eoff, R. L., and Raney, K. D. (2006) Intermediates revealed in the kinetic mechanism for DNA unwinding by a monomeric helicase. *Nat. Struct. Mol. Biol. 13*, 242–249.
30. Lucius, A. L., Wong, J. C., and Lohman, T. M. (2004) Fluorescence stopped-flow studies of single turnover kinetics of *E. coli* RecBCD helicase-catalyzed DNA unwinding. *J. Mol. Biol. 339*, 731–750.
31. Jankowsky, E., Gross, C. H., Shuman, S., and Pyle, A. M. (2000) The DExH protein NPH-II is a processive and directional motor for unwinding RNA. *Nature 403*, 447–451.
32. Levin, M. K., Wang, Y.-H., and Patel, S. S. (2004) The functional interaction of the hepatitis C virus helicase molecules is responsible for unwinding processivity. *J. Biol. Chem. 279*, 26005–26012.
33. Uemura, S., Kawaguchi, K., Yajima, J., Edamatsu, M., Toyoshima, Y. Y., and Ishiwata, S.'i. (2002) Kinesin-microtubule binding depends on both nucleotide state and loading direction. *Proc. Natl. Acad. Sci. U.S.A. 99*, 5977–5981.
34. Spudich, J. A. (2001) The myosin swinging cross-bridge model. *Nat. Rev. Mol. Cell Biol. 2*, 387–392.
35. Maluf, N. K., Fischer, C. J., and Lohman, T. M. (2003) A dimer of Escherichia *coli* UvrD is the active form of the helicase *in vitro*. *J. Mol. Biol. 325*, 913–935.
36. Ali, J. A., Maluf, N. K., and Lohman, T. M. (1999) An oligomeric form of *E. coli* UvrD is required for optimal helicase activity. *J. Mol. Biol. 293*, 815–834.
37. Ren, H., Dou, S.-X., Rigolet, P., Yang, Y., Wang, P.-Y., Amor-Gueret, M., and Xi, X. G. (2007) The arginine finger of the Bloom syndrome protein: its structural organization and its role in energy coupling. *Nucleic Acids Res. 35*, 6029–6041.
38. Singleton, M. R., Sawaya, M. R., Ellenberger, T., and Wigley, D. B. (2000) Crystal structure of T7 gene 4 ring helicase indicates a mechanism for sequential hydrolysis of nucleotides. *Cell 101*, 589–600.
39. Crampton, D. J., Guo, S., Johnson, D. E., and Richardson, C. C. (2004) The arginine finger of bacteriophage T7 gene 4 helicase: role in energy coupling. *Proc. Natl. Acad. Sci. U.S.A. 101*, 4373–4378.
40. Enemark, E. J., and Joshua-Tor, L. (2006) Mechanism of DNA translocation in a replicative hexameric helicase. *Nature 442*, 270–275.
41. Roman, L. J., Eggleston, A. K., and Kowalczykowski, S. C. (1992) Processivity of the DNA helicase activity of *Escherichia coli* recBCD enzyme. *J. Biol. Chem. 267*, 4207–4214.
42. Jezewska, M. J., and Bujalowski, W. (2000) Interactions of *Escherichia coli* replicative helicase PriA protein with single-stranded DNA. *Biochemistry 39*, 10454–10467.
43. Wong, I., and Lohman, T. M. (1992) Allosteric effects of nucleotide cofactors on *Escherichia coli* Rep helicase-DNA binding. *Science 256*, 350–355.
44. Jezewska, M. J., and Bujalowski, W. (1996) Global conformational transitions in *Escherichia coli* primary replicative helicase DnaB protein induced by ATP, ADP, and single-stranded DNA binding. *J. Biol. Chem. 271*, 4261–4265.
45. Hingorani, M. M., and Patel, S. S. (1993) Interactions of bacteriophage T7 DNA primase/helicase protein with single-stranded and double-stranded DNAs. *Biochemistry 32*, 12478–12487.
46. Kim, J. L., Morgenstern, K. A., Griffith, J. P., Dwyer, M. D., Thomson, J. A., Murcko, M. A., Lin, C., and Caron, P. R. (1998) Hepatitis C virus NS3 RNA helicase domain with a bound oligonucleotide: the crystal structure provides insights into the mode of unwinding. *Structure 6*, 89–100.
47. Velankar, S. S., Soultanas, P., Dillingham, M. S., Subramanya, H. S., and Wigley, D. B. (1999) Crystal structures of complexes of PcrA

DNA helicase with a DNA substrate indicate an inchworm mechanism. *Cell 97*, 75–84.
48. Levin, M. K., Gurjar, M., and Patel, S. S. (2005) A Brownian motor mechanism of translocation and strand separation by hepatitis C virus helicase. *Nat. Struct. Mol. Biol. 12*, 429–435.
49. Lee, J. Y., and Yang, W. (2006) UvrD helicase unwinds DNA one base pair at a time by a two-part power stroke. *Cell 127*, 1349–1360.
50. Dillingham, M. S., Wigley, D. B., and Webb, M. R. (2000) Demonstration of unidirectional single-stranded DNA translocation by PcrA helicase: measurement of step size and translocation speed. *Biochemistry 39*, 205–212.
51. Tomko, E. J., Fischer, C. J., Niedziela-Majka, A., and Lohman, T. M. (2007) A nonuniform stepping mechanism for *E. coli* UvrD monomer translocation along single-stranded DNA. *Mol. Cell 26*, 335–347.
52. Bernstein, D. A., Zittel, M. C., and Keck, J. L. (2003) High-resolution structure of the *E. coli* RecQ helicase catalytic core. *EMBO J. 22*, 4910–4921.
53. Zittel, M. C., and Keck, J. L. (2005) Coupling DNA-binding and ATP hydrolysis in *Escherichia coli* RecQ: role of a highly conserved aromatic-rich sequence. *Nucleic Acids Res. 33*, 6982–6991.
54. Korolev, S., Hsieh, J., Gauss, G. H., Lohman, T. M., and Waksman, G. (1997) Major domain swiveling revealed by the crystal structures of complexes of *E. coli* Rep helicase bound to single-stranded DNA and ADP. *Cell 90*, 635–647.
55. Theissen, B., Karow, A. R., Köhler, J., Gubaev, A., and Klostermeier, D. (2008) Cooperative binding of ATP and RNA induces a closed conformation in a DEAD box RNA helicase. *Proc. Natl. Acad. Sci. U.S.A. 105*, 548–553.
56. Skordalakes, E., and Berger, J. M. (2006) Structural insights into RNA-dependent ring closure and ATPase activation by the Rho termination factor. *Cell 127*, 553–564.
57. Büttner, K., Nehring, S., and Hopfner, K.-P. (2007) Structural basis for DNA duplex separation by a superfamily-2 helicase. *Nat. Struct. Mol. Biol. 14*, 647–652.